Quasi-Static Characteristics of Microstrip on an Anisotropic Sapphire Substrate

ROGER P. OWENS, JAMES E. AITKEN, AND TERENCE C. EDWARDS

Abstract—**The well-defined and repeatable electrical properties of single-crystal sapphire make it an attractive substrate material for microstrip, but its dielectric anisotropy constitutes an important design complication. This paper describes investigations into the quasi-static characteristics of single microstrip lines on sapphire substrates cut with a specified orientation. To account for anisotropy, a new permittivity parameter ε_{req} is introduced, which is a function of the linewidth to substrate-height ratio W/h. The variation of ε_{req} with W/h is derived by finite-difference methods. Universal curves for microstrip on correctly orientated sapphire are presented, showing 1) ε_{req}, 2) the low-frequency limit of effective microstrip permittivity ε_{e0}, and 3) the characteristic impedance of the line Z_0, all as functions of W/h.**

I. Introduction

THE PERMITTIVITY of nominally identical alumina-ceramic substrates is known to vary significantly from batch to batch. New-batch measurement thus becomes necessary to determine the permittivity parameter needed for subsequent design of microstrip circuitry. One important advantage of single-crystal sapphire substrates is that such repeated measurement is unnecessary because the sapphire has well-defined and repeatable electrical properties. Being uniaxial, however, the crystal is anisotropic, and has a permittivity parallel to the optical axis (C axis) $\varepsilon_0\varepsilon_\parallel$, which is higher than the permittivity in the plane perpendicular to this axis, $\varepsilon_0\varepsilon_\perp$. Sapphire substrates are therefore usually cut with their plane surfaces perpendicular to the C axis so that the material permittivity is constant everywhere in the plane of the substrate. A propagating wave traveling along a microstrip line on the substrate is then not subjected to a change in permittivity at bends or corners in the line. The purpose of this paper is to determine the effect of this specified anisotropy on the quasi-static characteristics of microstrip lines deposited on the substrate. We will show that the magnitude of this effect is of practical significance. The microwave performance of the lines will also be influenced by dispersion, and experimental investigations into this aspect of the behavior of microstrip on sapphire are reported in another paper [1].

The substrate geometry and coordinate designation are shown in Fig. 1. We examine the case when the C axis corresponds to the y-coordinate in this figure. The principal relative permittivities of sapphire are chosen to be

$$\varepsilon_\perp = \varepsilon_x = \varepsilon_z = 9.40 \qquad \varepsilon_\parallel = \varepsilon_y = 11.60.$$

This choice of values is considered further in Section II.

Manuscript received September 15, 1975; revised January 26, 1976.
The authors are with the Department of Electrical and Electronic Engineering, Royal Military College of Science, Shrivenham, Swindon, Wilts., England.

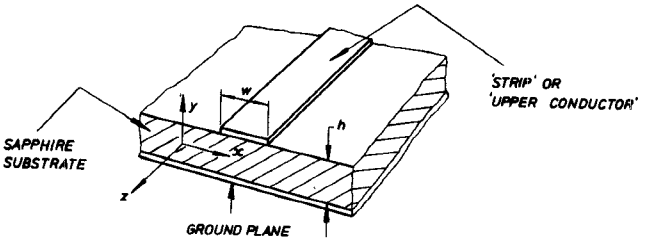

Fig. 1. Microstrip on sapphire (C axis perpendicular to ground plane).

The well-defined anisotropy enables us to specify for sapphire a unique linewidth-dependent permittivity parameter which we term the equivalent isotropic-substrate relative permittivity ε_{req}. This is defined as the permittivity of an isotropic substrate, supporting a microstrip line, which would yield microstrip parameters such as line capacitance per meter C, impedance Z_0, and effective microstrip permittivity ε_{e0} (low-frequency limiting value), which are identical to those of the same line on sapphire. For a given linewidth, the appropriate ε_{req} value may then be used as the material permittivity in any microstrip design equations. Clearly, for wide lines the electric field immediately under the strip will predominate, and it will lie largely in the y direction. Thus ε_{req} will approach ε_y for large W/h. As the lines become narrower, the permittivity component ε_x will have greater effect, and ε_{req} will steadily fall to some intermediate value between ε_x and ε_y. The following sections describe how the variations of ε_{req}, ε_{e0}, and Z_0 with W/h have been determined for microstrip lines on the specified sapphire substrate.

II. The Principal Relative Permittivities of Sapphire

The most recent accurate determination of sapphire relative permittivities appears to be that reported by Fontanella *et al.* [2], who quote the values $\varepsilon_\perp = 9.395 \pm 0.005$, and $\varepsilon_\parallel = 11.589 \pm 0.005$. The measurements were made at a frequency of 1 kHz. Loewenstein *et al.* [3] report results obtained from extrapolated infrared refractive-index measurements, quoting $\varepsilon_\perp = 9.413 \pm 0.008$ and $\varepsilon_\parallel = 11.601 \pm 0.008$.

Measurements specifically in the microwave frequency band 2–12 GHz were recently made by Ladbrooke *et al.* [4], who quote $\varepsilon_\perp = 9.34$, $\varepsilon_\parallel = 11.49$, both with ± 0.5-percent error bands. These results were not corrected for the finite Q factor of the resonators [5], neither were the "magnetic side-wall" resonator measurements corrected for fringing fields along the open edge [6]. Appendix A discusses how Q and capacitive fringing corrections may be made. Lack of precise fringing capacitance information for the particular

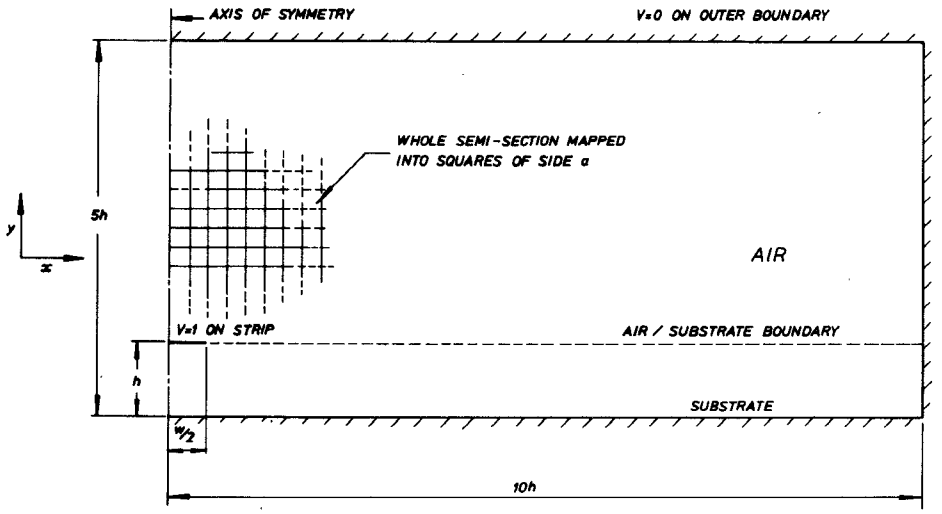

Fig. 2. Geometry of the computer solution.

geometry of the substrates precludes accurate recalculation of their permittivities, but it is concluded that the mean values for each orientation are about 0.5 percent higher than those given in [4], and the results from [2] and [3] lie well within the new error bounds. The infrared results [3] indicate that there is less than 0.1-percent bulk material dispersion in sapphire below 300 GHz, so the choice of $\varepsilon_\perp = 9.40$ and $\varepsilon_\parallel = 11.60$ for the present work is well justified. Based on the errors quoted in [2] and [3], error bounds of ± 0.01 are estimated for each of these values.

III. Outline of Finite-Difference Computations

The finite-difference method [7]–[10] has been used to compute theoretical values for the quasi-static line capacitances per meter of microstrip lines on anisotropic substrates with selected principal permittivity components over the range $0.125 \leq W/h \leq 9$. Implicit in the finite-difference solution is the assumption that the propagating waves on microstrip are TEM waves. This assumption is only satisfactory at the low-frequency (LF) limit and other theories should be used to take into account dispersion effects [11], [12]. At the LF limit the impedance and effective permittivity associated with a given microstrip line may be derived from the line capacitance values using simple TEM relationships. Alternatively, an interpolation technique, described later, may be used to deduce ε_{req} directly from line capacitance computations for both isotropic and anisotropic permittivity tensors.

Fig. 2 depicts the geometry of the semisection from which we obtain the computer solution for the case $W/h = 1$. The boundaries are removed sufficiently far from the strip that the computed solutions are virtually independent of boundary positions. The relative effects of side wall and top wall on the computed capacitances depend on the width of the strip. For wide strips the relative position of the side wall is important, while for narrow strips the location of the top wall has greater effect. Fig. 2 also illustrates the coarsest net employed, which corresponds to four elemental squares across the thickness h of the substrate. A factor N is used in the computation to generate a new net which is finer, by the same factor, than that shown in Fig. 2. The substrate is then $4N$ squares high and the side walls $40N$ squares away from the axis of symmetry. In general, the highest value of N used was $N = 7$, but for the case $W/h = 0.125$ we used $N = 12$, which provides 6 elemental squares along the narrow strip. Computations in general follow the standard relaxation methods for the solution of the potential at each net point [9], but special finite-difference equations are required to account for the anisotropy of the substrate. The three finite-difference equations used for net points 1) entirely on the substrate, 2) entirely in air, and 3) on the air/substrate boundary, are derived in Appendix B [(B7)–(B9)]. All node potentials within the boundaries are initially at estimated values, and the left side of the appropriate finite-difference equation is evaluated. Equation (B9) of Appendix B, for example, will yield a residual potential $R = \frac{1}{4}(V_B + V_D + V_E + V_C) - V_A$. Each potential in the net is replaced at the nth iterative scanning of the net by an updated potential $V(n) = V(n-1) + \alpha R$, where the overrelaxation factor α was chosen to be around 1.8.

The magnitude of the normal electric field E_n at each node on the strip is computed from the potentials on adjacent nodes, and the line capacitance per meter is obtained from the surface integral (taken over a length of 1 m) of the normal electric flux density, i.e.,

$$C = \varepsilon_0 \iint_S \varepsilon_n E_n \, dS.$$

The normal relative permittivity ε_n has the value unity along the top surface of the strip, and ε_y along the bottom surface. We have taken an average value $\frac{1}{2}(1 + \varepsilon_x)$ normal to the two edges, which is justified by (B8) in Appendix B.

Theoretical estimation of the accuracy of a single finite-

TABLE I

W/h	9.0	4.0	2.0	1.0	0.5	0.25	0.125
ε_{req}	11.50	11.40	11.27	11.10	10.96	10.89	10.80
ε_{eo}	9.718	8.806	8.027	7.391	6.965	6.712	6.522
Z_o Ω	10.17	19.51	31.50	46.60	63.26	80.36	97.76

Note: $\varepsilon_x = 9.40$, $\varepsilon_y = 11.60$.

TABLE II

W/h		9.0	4.0	2.0	1.0	0.5	0.25	0.125
Change in ε_{req} for 0.1 change in (1) ε_x, (2) ε_y	(1)	0.010	0.010	0.015	0.025	0.030	0.035	0.035
	(2)	0.090	0.090	0.085	0.075	0.070	0.065	0.065

difference solution is very difficult, and in the present work the following procedure has been adopted in order to improve the accuracy of the final solution. For each net the capacitance per meter is computed and printed out every 15 iterations until it is found to change by less than 0.1 percent. A final capacitance value for the net is then estimated by extrapolation. The final values for successively finer nets are used, in a similar way, to estimate the capacitance C_∞ that would be computed on an infinitely fine net. This stage is carried out graphically, by plotting C against $\exp(N_{max} - N)$ and observing where the smooth curve through the points intercepts the C axis where $\exp(-\infty) = 0$.

The asymptotic value of capacitance is reached fairly rapidly for $W/h \geq 1$, but below this value the successive final capacitances for each net do not converge quickly, and the asymptotic capacitance becomes progressively more difficult to estimate. This difficulty extends to the higher W/h ratios when the capacitance C_1 for air dielectric is computed. However, it was not the intention to calculate Z_0 and ε_{e0} directly from computations of C and C_1, so this approach was not pursued. Instead, the parameter ε_{req} was calculated as follows from computations of C alone. For each W/h, capacitances C_a and C_b were computed for isotropic substrates with relative permittivities ε_a and ε_b just above and below the predicted ε_{req} value, and ε_{req} was calculated using the interpolation formula

$$\varepsilon_{req} = \varepsilon_b + (\varepsilon_a - \varepsilon_b) \cdot (C - C_b)/(C_a - C_b).$$

Better convergence and accuracy would be achieved if a graded mesh were used, involving a fine net near the strip, increasing to a coarse net near the conducting boundaries. A more advanced version of the program is being written to incorporate this refinement, which is necessary when using the finite-difference technique for analysis of closely spaced coupled lines.

IV. Computed Results

Table I shows the results obtained theoretically for the relative permittivities $\varepsilon_x = 9.40$, $\varepsilon_y = 11.60$. The figures for the LF limit of effective microstrip permittivity ε_{e0} and the characteristic impedance Z_0 were obtained from the W/h and ε_{req} data using a computer program based upon the theory of Bryant and Weiss [13].

The error bounds on these results are dictated by the limitations of the computer core store, because the N-factor previously mentioned has to be traded off against the size of the box defining the boundary walls. For $W/h < 1$, the error in estimating the asymptotic capacitance increased due to slow convergence. It was possible to increase N to 12 for the narrowest line, $W/h = 0.125$, without sacrificing accuracy due to insufficient box size, but convergence was still poor, and an error of about 0.5 percent in predicting C_∞ was estimated. At the other end of the scale, although convergence was rapid for the line $W/h = 9.0$, the results were sensitive to box size. By using the largest box consistent with maintaining an adequately high N-factor, again a probable error of ± 0.5 percent was achieved. The estimated error on the results for the middle value, $W/h = 1$, was down to ± 0.2 percent.

Calculations of ε_{req} were also made for slightly different ε_x and ε_y values, to determine its sensitivity to these parameters. Table II indicates how much ε_{req} is altered by changes of 0.1 in ε_x and ε_y, respectively.

V. Discussion of Results

The computation of each ε_{req} value using the finite-difference method is a lengthy process, and because of the net structure used, only a limited number of W/h ratios can be chosen for solution. For computer-aided design purposes, it is necessary to derive either an analytical equation or a readily analyzable semiempirical model for microstrip on an anisotropic substrate, by curve fitting to the existing points. Both approaches were tried. The equation

$$\varepsilon_{req} = 12.0 - \frac{1.21}{1 + 0.39[\log(10W/h)]^2} \qquad (1)$$

results in curve *a* of Fig. 3, which fits the finite-difference points very well in the range $0.1 \leq W/h \leq 10.0$. The numerical terms in this equation are purely empirical,

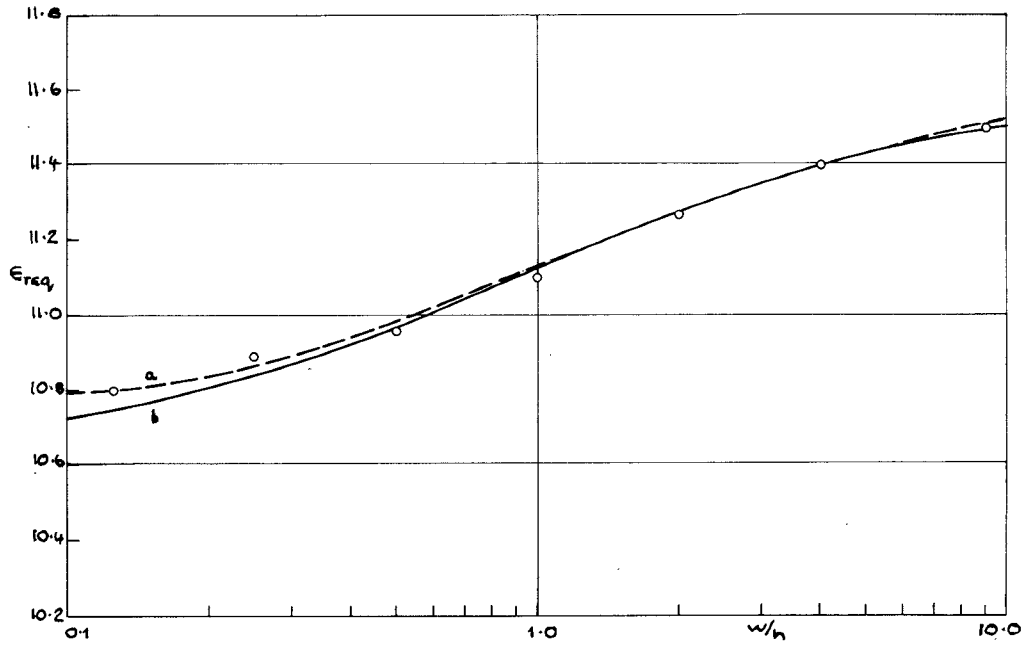

Fig. 3. Equivalent relative permittivity versus W/h for microstrip lines on a sapphire substrate (C axis perpendicular to ground plane), with $\varepsilon_\perp = 9.40$, $\varepsilon_\parallel = 11.60$. ○—Theoretical points (finite-difference bomputation). Curve a from (1). Curve b using microstrip model (Appendix C).

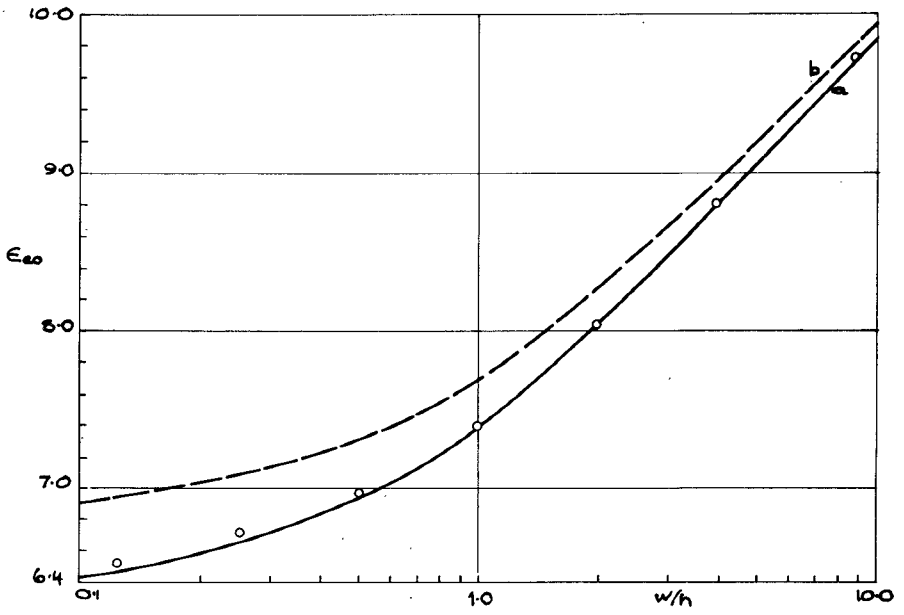

Fig. 4. Effective microstrip permittivity versus W/h for microstrip on a sapphire substrate (C axis perpendicular to ground plane). Curve a: $\varepsilon_i = 10.60$, $\varepsilon_y = 11.60$. Curve b: isotropic substrate with $\varepsilon_r = 11.60$.

however, whereas the approximate microstrip model described in Appendix C reduces the degree of empiricism to a single permittivity value ε_i. Curve b of Fig. 3 is generated when ε_i is chosen to be 10.60.

The fit is very good until W/h falls below 0.5, into the region where the error in the theoretical points is greater and the model is less likely to correspond to the actual situation. Nevertheless, this result justifies the use of a model which is clearly not exact, but behaves very similarly to the actual microstrip.

Curve a of Fig. 4 shows the corresponding variation of ε_{e0} with W/h, with points from Table I superimposed. The error in the derived value of the material permittivity which would result if anisotropy were neglected and a fixed value of 11.60 were used is obvious from Fig. 3. The corresponding error that would arise in ε_{e0} can be deduced by comparing curve a of Fig. 4 with curve b, which is applicable to an isotropic substrate with $\varepsilon_r = 11.60$. Fig. 5 shows the calculated relationship between Z_0 and W/h for sapphire, taking into account the variation in ε_{req}, and again points from Table I are added. In this case, the particular value of ε_{req} is not so critical, but if a fixed value of 11.6 were used

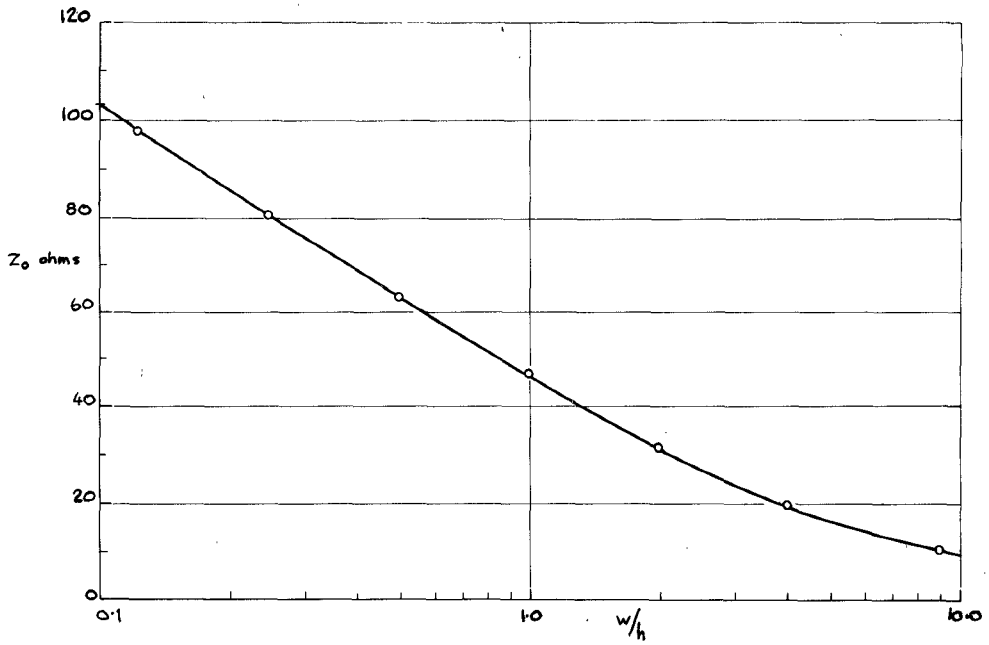

Fig. 5. Impedance versus W/h for microstrip on a sapphire substrate (C axis perpendicular to ground plane).

the error in Z_0 would be -4 percent for $W/h = 0.1$ falling to -0.5 percent at $W/h = 1.0$. Figs. 4 and 5 represent universal curves for determining the quasi-static parameters of single microstrip lines on a sapphire substrate cut in the plane specified by Fig. 1.

VI. Conclusions

This paper has primarily dealt with sapphire substrates cut with their plane surfaces perpendicular to the crystal C axis, although the theoretical methods are applicable to other orientations. Likewise, the methods can be applied to coupled lines, although single microstrip lines only are considered here. The effect of substrate anisotropy on the behavior of single microstrip lines on these substrates has been accounted for by introducing a new linewidth-dependent permittivity parameter ε_{req}. This is so defined that it can be used as the conventional (isotropic) substrate permittivity in any microstrip design equations. The variation of ε_{req} with W/h has been derived theoretically using a finite-difference method. An empirical equation and a nonrigorous model for microstrip on an anisotropic substrate have been employed to enable ε_{req} to be calculated for any required W/h in the range $0.1 \leq W/h \leq 10.0$ without further recourse to the finite-difference computations. In addition, the model has been used to generate universal curves of ε_{e0} and Z_0 versus W/h for microstrip on sapphire substrates with the specified orientation.

Appendix A

A. Reexamination of the Results of [4]

Ladbrooke *et al.* [4] measured the resonant frequencies of both wholly and partly metallized sapphire substrates cut with the C axis either parallel or perpendicular to the large surfaces of the slice. The permittivities were then deduced from the equation

TABLE III

Resonator types	Mean permittivity values	
	$\varepsilon_\perp$	$\varepsilon_\parallel$
Metallised-edge, All modes	9.59	11.80
Open-edge, (n, o) modes	9.34	11.49
Open edge, (n, m) modes, m ⩾ 1	9.13	11.24

$$\varepsilon_y = \left(\frac{c}{2lf_{n,m}}\right)^2 \cdot (n^2 + m^2) \tag{A1}$$

where c is the velocity of light, ε_y is the permittivity in the direction y defined in Fig. 1, l is the length of side of the square substrate, and n,m are mode numbers. The results were as shown in Table III. From an analysis of coupling errors, it was argued [4] that the open-edge $(n,0)$ mode resonator results were within 0.5 percent of the true permittivities. Howell [5], [6], however, pointed out that further corrections to these results are necessary to account for radiation loss and fringing at the open edge of the resonators.

Losses cause a downward shift in resonant frequency of $\Delta f/f = 1/2Q$, where Q is the loaded Q factor of the resonator [5], [18]. Correction for this leads to a smaller result for ε_y by the factor $\Delta\varepsilon/\varepsilon_y = 2\Delta f/f = 1/Q$ according to (A1). Q's approaching 200 and above were measured for $(n,0)$ modes in open-edge resonators, indicating a correction of well below 1 percent.

Failure to allow for electric fringing fields present at the edges of the substrate results in a calculated value of ε_y which is lower than the true value. Correction in this case thus has the reverse effect to the Q correction. There appears to be no analysis in the literature dealing with the fringing effects of parallel-plate resonators with an air–dielectric interface around the open edge of the resonator. However, it was felt that the static analysis of the appropriate dielectric-filled configuration would provide some

indication of the magnitude of the correction required. Reference [15] alone deals with this situation, but it is difficult to estimate the fringing capacitance relevant to the small ratio $h/l = 0.02$ which applies to our substrates. Moreover, there is some doubt about the accuracy of results from [15], because although the estimated fringing capacitance for the completely air-filled system agrees fairly well with [16], it is five times that predicted by [17]. Until further information becomes available, preferably for the resonator rather than the static capacitor, no firm conclusions about fringing corrections can be made. It is only possible to say that the $(n,0)$ mode results of [4] seem to mark a lower bound to the true permittivity results.

The metallized-edge resonator results do not require any correction for fringing or loss (Q's well in excess of 400 were measured for our completely metallized substrates), but it is known that because of coupling errors they represent an upper bound to the true values [4].

Based on the figures of Table III, therefore, we conclude that the microwave measurements of [4] establish the principal relative permittivities of sapphire as $\varepsilon_\perp = 9.47 \pm 0.13$, and $\varepsilon_\parallel = 11.64 \pm 0.16$. The tolerances quoted here would almost certainly be reduced if the corrections outlined above were quantified and taken into account.

Appendix B

A. Permittivity Tensor for Sapphire of Suitable Orientation

The permittivity tensor of an anisotropic crystal with its principal axes coincident with the coordinate system axes, is the diagonal matrix shown in the following equation, which relates the electric displacement vector $\boldsymbol{D}$ to the electric field $\boldsymbol{E}$ [18]

$$\boldsymbol{D} = \begin{bmatrix} \varepsilon_x & 0 & 0 \\ 0 & \varepsilon_y & 0 \\ 0 & 0 & \varepsilon_z \end{bmatrix} \varepsilon_0 \boldsymbol{E}.$$

Sapphire is a uniaxial crystal, and our substrates are cut such that ε_y coincides with its C axis. Hence $\varepsilon_y = \varepsilon_\parallel$ and $\varepsilon_x = \varepsilon_z = \varepsilon_\perp$. In the quasi-TEM theory, $E_z = 0$, therefore,

$$\boldsymbol{D} = i\varepsilon_0\varepsilon_x E_x + j\varepsilon_0\varepsilon_y E_y. \tag{B1}$$

B. Special Finite-Difference Equations

Consider conditions at the interface between two different anisotropic dielectrics with their principal axes aligned with the coordinate system. Assume the net point A is located on the interface, at coordinates (x,h) and points B, C, D, and E are located distances a from point A as shown in Fig. 6. In charge-free space $\nabla \cdot \boldsymbol{D} = 0$. Therefore, in the upper dielectric $(y > h)$

$$\varepsilon_x' \frac{\partial^2 V(x,y)}{\partial x^2} + \varepsilon_y' \frac{\partial^2 V(x,y)}{\partial y^2} = 0 \tag{B2}$$

and in the lower dielectric $(0 < y < h)$

$$\varepsilon_x \frac{\partial^2 V(x,y)}{\partial x^2} + \varepsilon_y \frac{\partial^2 V(x,y)}{\partial y^2} = 0 \tag{B3}$$

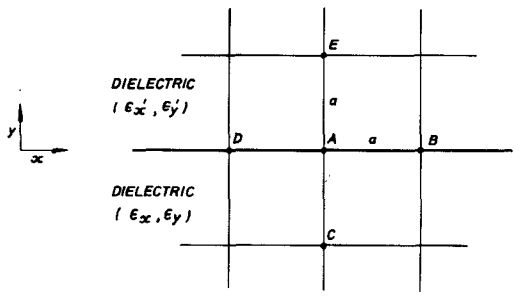

Fig. 6. Net points around point A on anisotropic dielectric interface.

where $\varepsilon_x', \varepsilon_y'$ are values for the upper dielectric and $\varepsilon_x, \varepsilon_y$ for the lower.

At the interface $(y = h)$ the tangential field $-(\partial V/\partial x)$ and its gradient $-(\partial^2 V/\partial x^2)$ must be continuous across the boundary for all values of x. For example,

$$\frac{\partial^2 V(x, h - \delta y)}{\partial x^2} = \frac{\partial^2 V(x, h + \delta y)}{\partial x^2} = \frac{\partial^2 V(x,h)}{\partial x^2}. \tag{B4}$$

Here, $\delta y \to 0$ and is used to indicate y-coordinates just inside and just outside the interface.

In addition, the normal component of $\boldsymbol{D}$ must be continuous across the interface, i.e.,

$$\varepsilon_y \frac{\partial V(x, h - \delta y)}{\partial y} = \varepsilon_y' \frac{\partial V(x, h + \delta y)}{\partial y}. \tag{B5}$$

The net point potentials V_B, V_C, V_D, V_E are obtained in terms of V_A and the appropriate partial derivatives of V by applying Taylor's theorem in the normal way [7]–[10]. Elimination of all partial derivatives using (B2)–(B5) results in the following general finite-difference equation:

$$\tfrac{1}{2}(\varepsilon_x' + \varepsilon_x)(V_B + V_D) + \varepsilon_y' V_E + \varepsilon_y V_C - (\varepsilon_x' + \varepsilon_x + \varepsilon_y' + \varepsilon_y)V_A = 0. \tag{B6}$$

In the present problem this is reduced to three special cases.

Case 1: $0 < y < h$: All net points lie within the lower dielectric material; thus $\varepsilon_y' = \varepsilon_y$ and $\varepsilon_x' = \varepsilon_x$ and (B6) becomes

$$\varepsilon_x(V_B + V_D) + \varepsilon_y(V_E + V_C) - 2(\varepsilon_x + \varepsilon_y)V_A = 0. \tag{B7}$$

Case 2: $y = h$: The upper dielectric is air; i.e., $\varepsilon_y' = \varepsilon_x' = 1$ and (B6) becomes

$$\tfrac{1}{2}(1 + \varepsilon_x)(V_B + V_D) + V_E + \varepsilon_y V_C - (2 + \varepsilon_x + \varepsilon_y)V_A = 0. \tag{B8}$$

Case 3: $y > h$: All net points lie in air; i.e., $\varepsilon_y' = \varepsilon_y = \varepsilon_x' = \varepsilon_x = 1$ and (B6) becomes

$$V_B + V_D + V_E + V_C - 4V_A = 0. \tag{B9}$$

Appendix C

A. Simple Model for Microstrip on the Anisotropic Substrate

The major effect of the substrate anisotropy occurs beneath the strip where the electric field is primarily in the y direction, so that the component ε_x makes very little

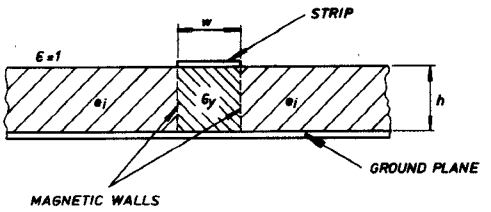

Fig. 7. Model for microstrip on an anisotropic substrate (C axis perpendicular to ground plane).

contribution to the capacitance in this region. Elsewhere in the substrate and in the air above it, the direction and density of the electric flux is such that ε_y and ε_x have about equal influences on the remaining capacitance associated with the microstrip. It is reasonable to assume, therefore, that the hypothetical structure of Fig. 7 would behave in a very similar way to the microstrip under investigation. In this model, magnetic walls exist in the dielectric region only, in the constant x planes situated at each edge of the strip, so that the electric field under the strip lies entirely in the y direction. Between the magnetic walls the dielectric has the permittivity ε_y. Outside these walls, the substrate has an isotropic relative permittivity ε_i which is a linear combination of ε_x and ε_y, that is: $\varepsilon_i = b\varepsilon_y + (1 - b)\varepsilon_x$, where ε_i and hence b are in general expected to be functions of W/h.

The total capacitance C per unit length of the microstrip model thus consists of the parallel-plate capacitance beneath the strip $C_p = \varepsilon_y\varepsilon_0 W/h$, and the fringing capacitance C_f arising from electric flux lines originating from the top surface and edges of the strip. C_f will be approximately equal to the difference between the total capacitance of conventional microstrip on an isotropic substrate of permittivity ε_i (which can be calculated for any required W/h using Wheeler [14], or other analysis theories) and the parallel-plate capacitance previously defined, with ε_i replacing ε_y. The equivalent relative permittivity ε_{req} is then given by a combination of ε_i and ε_y weighted by the respective capacitance ratios C_f/C and C_p/C; i.e.,

$$\varepsilon_{req} = \varepsilon_i \cdot \frac{C_f}{C} + \varepsilon_y \cdot \frac{C_p}{C}$$

$$= \frac{\varepsilon_i C_f + \varepsilon_y C_p}{C_f + C_p}.$$

Use of this ε_{req} in Wheeler or other analysis processes will give Z_0 and ε_{e0} also as functions of W/h.

It was found that ε_{req} calculated in this way using a constant value of ε_i independent of W/h corresponded very closely with the finite-difference theory values of ε_{req}. An optimized value $\varepsilon_i = 10.60$ was obtained by curve fitting to the finite-difference theory points given in Table I, as shown in Fig. 3.

Acknowledgment

The authors wish to thank Prof. M. H. N. Potok, who directs the MIC research program, of which this work is a part, for useful discussions and recommendations. Helpful correspondence with Dr. P. H. Ladbrooke is acknowledged.

References

[1] T. C. Edwards and R. P. Owens, "2–18-GHz dispersion measurements on 10–100-Ω microstrip lines on sapphire," this issue, pp. 506–513.
[2] J. Fontanella, C. Andeen, and D. Schuele, "Low-frequency dielectric constants of α-quartz, sapphire, MgF_2 and MgO," *J. Appl. Phys.*, vol. 45, no. 7, pp. 2852–2854, July 1974.
[3] E. V. Loewenstein, D. R. Smith, and R. L. Morgan, "Optical constants for infra-red materials. 2: Crystalline solids," *Appl. Optics*, vol. 12, pp. 398–406, Feb. 1973.
[4] P. H. Ladbrooke, M. H. N. Potok, and E. H. England, "Coupling errors in cavity-resonance measurements on MIC dielectrics," *IEEE Trans. Microwave Theory and Tech.*, vol. MTT-21, pp. 560–562, August 1973.
[5] J. Q. Howell, "A quick accurate method to measure the dielectric constant of microwave integrated-circuit substrates," *IEEE Trans. Microwave Theory and Tech.*, vol. MTT-21, pp. 142–143, March 1973.
[6] P. H. Ladbrooke, M. H. N. Potok, E. H. England, and Reply by J. Q. Howell, "Comments on 'A quick accurate method to measure the dielectric constant of microwave integrated-circuit substrates,'" *IEEE Trans. Microwave Theory and Tech.*, vol. MTT-21, pp. 570–571, August 1973.
[7] H. E. Green, "The numerical solution of some important transmission-line problems," *IEEE Trans. Microwave Theory and Tech.*, vol. MTT-13, pp. 676–692, Sept. 1965.
[8] M. V. Schneider, "Computation of impedance and attenuation of TEM-lines by finite difference methods," *IEEE Trans. Microwave Theory and Tech.*, vol. MTT-13, pp. 793–800, November 1965.
[9] H. E. Stinehelfer, "An accurate calculation of uniform microstrip transmission-lines," *IEEE Trans. Microwave Theory and Tech.*, vol. MTT-16, pp. 439–447, July 1968.
[10] D. H. Sinnott, G. K. Cambrell, C. T. Carson, and H. E. Green, "The finite difference solution of microwave circuit problems," *IEEE Trans. Microwave Theory and Tech.*, vol. MTT-17, pp. 464–477, August 1969.
[11] E. J. Denlinger, "A frequency dependent solution for microstrip transmission lines," *IEEE Trans. Microwave Theory and Tech.*, vol. MTT-19, pp. 30–39, January 1971.
[12] T. Itoh and R. Mittra, "Spectral-domain approach for calculating the dispersion characteristics of microstrip lines," *IEEE Trans. Microwave Theory and Tech.*, vol. MTT-21, pp. 496–499, July 1973.
[13] T. C. Cisco, "Design of microstrip components by computer," NASA Contractor Report CR-1982, March 1972, Program C267.
[14] H. A. Wheeler, "Transmission-line properties of parallel strips separated by a dielectric sheet," *IEEE Trans. Microwave Theory and Tech.*, vol. MTT-13, pp. 172–188, March 1965.
[15] A. T. Adams and J. R. Mautz, "Computer solution of electrostatic problems by matrix inversion," *Proc. Nat. Electron. Conf. 1969*, pp. 198–201.
[16] D. K. Reitan, "Accurate determination of the capacitance of rectangular parallel-plate capacitors," *J. Appl. Phys.*, vol. 30, no. 2, pp. 172–176, Feb. 1959.
[17] R. F. Harrington, *Field Computation by Moment Methods.* New York: Macmillan, 1968, p. 34.
[18] R. E. Collin, *Foundations for Microwave Engineering.* New York: McGraw-Hill, 1966.